Journal of Magnetic Resonance **141,** 340–346 (1999)
Article ID jmre.1999.1924, available online at http://www.idealibrary.com on IDEAL®

Asymmetric MRI Magnet Design Using a Hybrid Numerical Method

Huawei Zhao, Stuart Crozier,[1] and David M. Doddrell

Centre for Magnetic Resonance, The University of Queensland, St. Lucia, Brisbane, Queensland 4072, Australia

Received May 5, 1999; revised August 30, 1999

This paper describes a hybrid numerical method for the design of asymmetric magnetic resonance imaging magnet systems. The problem is formulated as a field synthesis and the desired current density on the surface of a cylinder is first calculated by solving a Fredholm equation of the first kind. Nonlinear optimization methods are then invoked to fit practical magnet coils to the desired current density. The field calculations are performed using a semi-analytical method. A new type of asymmetric magnet is proposed in this work. The asymmetric MRI magnet allows the diameter spherical imaging volume to be positioned close to one end of the magnet. The main advantages of making the magnet asymmetric include the potential to reduce the perception of claustrophobia for the patient, better access to the patient by attending physicians, and the potential for reduced peripheral nerve stimulation due to the gradient coil configuration. The results highlight that the method can be used to obtain an asymmetric MRI magnet structure and a very homogeneous magnetic field over the central imaging volume in clinical systems of approximately 1.2 m in length. Unshielded designs are the focus of this work. This method is flexible and may be applied to magnets of other geometries. © 1999 Academic Press

Key Words: **MRI magnet; asymmetric design; hybrid numerical method.**

A major specification of the static field in magnetic resonance imaging (MRI) is that it has to be homogeneous over the diameter spherical imaging volume (dsv). The errors are usually less than 10 ppm rms over a 45–50 cm dsv. Conventional medical MRI systems are typically around 1.6–2.0 m in length with free bore diameters in the range 0.8–1.0 m (*1–15*). Normally, the magnet is symmetric and dsv is located in the geometric center of the structure. Many of the early magnet designs, in theory, were based on the work of Garrett (*1–3*). Recently, a stochastic optimization technique was successfully used to design symmetric, compact MRI magnets (*14*).

In this work, the primary objective was to develop new designs for compact asymmetric MRI magnet structures, so that the dsv region could be located as close as possible to one end of magnet. The main advantages of making the magnet asymmetric include the potential to reduce the perception of claustrophobia for the patient, better access to the patient by attending physicians, and the potential for reduced peripheral nerve stimulation due to the gradient coil configuration. The constraints placed on the new magnet were that the overall length of the magnet be less than 1.25 m with a free bore of about 1.0 m and the dsv at about 0.1 m from the end of the magnet coils. Furthermore, the design must ensure suitable safety margins for the use of niobium–titanium superconductors and generate 1.0 T with suitable homogeneity over at least a 45 cm dsv.

The challenge in designing a compact asymmetric magnet is the retention of high homogeneity conditions over the imaging volume, as magnet homogeneity is strongly dependent on the overall length of the coil structure. Another parameter strongly affecting homogeneity is the relaxation factor ($\gamma = \mathbf{d}/\mathbf{R}$) (see Fig. 1) that defines as a ratio the distance (**d**) from the end of the coil to the beginning of the dsv on axis with free bore radius (**R**). Consequently, the smaller γ, the more difficult it is to obtain the homogeneity requirements in the dsv.

In this paper, a new hybrid numerical method is proposed to determine the final coil design. The method combines the inverse current density approach previously used in gradient (*16, 17*) and shim coil (*18*) designs and nonlinear optimization numerical techniques. The field calculation is performed by a semi-analytical method, which has been developed by Forbes *et al.* (*20*). It is well known that there is no unique solution for a particular magnet structure; therefore, an inverse approach by a current density method was used to find a suitable current density profile for a specified total magnet length, dsv size and position, and required field strength. This distribution is used as a starting point for the coil block design, and then a nonlinear optimization method is used to refine the configuration of the magnet. The primary objective was to develop new designs for compact asymmetric MRI magnet structures with relaxation factors $\gamma \leq 0.20$, so that the dsv region could be located as close as possible to the one end of magnet.

The first step in the design process is to find the source current density, which is constrained to the surface of a cylinder of fixed length. The current density **J**, which must produce a homogeneous magnetic field over the dsv, can be related to specific magnetic field distribution by an integral equation obtained from the Biot–Savart law (*19*). In a conventional MRI magnet design, the problem is presented as Fig. 1, an air-cored coil with an infinitely thin winding tape carrying current. The integral equation has the expression

[1] To whom correspondence should be addressed. E-mail: stuart.crozier@cmr.uq.edu.au.

1090-7807/99 $30.00

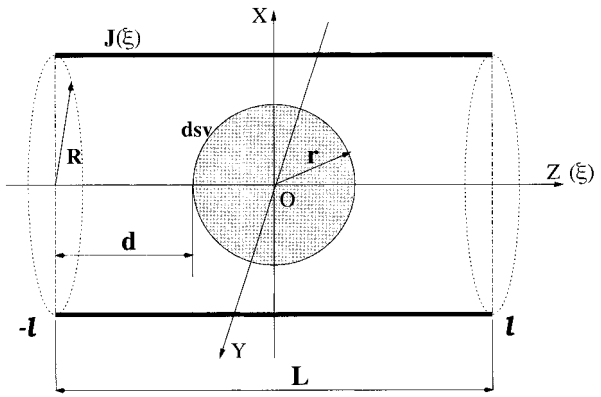

FIG. 1. An air-cored coil with an infinitely thin current density layer in a fully symmetric magnet system.

$$\int_{-l}^{l} K(z, \xi)\mathbf{J}(\xi)d\xi = B_z. \qquad [1]$$

For computational efficiency, this approach only considers the magnetic field distribution along the Z-axis. Therefore, the kernel function is $K(z, \xi) = \mu_0 R^2/(2(R^2 + (z - \xi)^2)^{3/2})$. Equation [1] is a linear Fredholm integral equation of the first kind, which can be represented by the discrete system of algebraic equations

$$\sum_{i=1}^{n} A_{ji}J_i = B_{zj}, \quad j = 1, 2, \ldots, m, \qquad [2]$$

where A_{ji} is a $m \times n$ matrix which is generated from the kernel function. When $m > n$, there is more information than unknowns and the problem is over specified.

In general, numerical solution of [2] is a difficult task, because this problem belongs to the class of so-called ill-posed problems, and direct solution of the system generally yields a vector **J** whose components will oscillate wildly around the corresponding values of the solution of [1]. A special numerical technique is required, and here we present brief details of the asymptotic regularization method (*22*). A general regularized solution **J** is given by the solution of the following optimization problem:

$$\min\|\mathbf{AJ} - \mathbf{B}_z\|^2. \qquad [3]$$

The direct solution of [3] is generally numerically unstable. Asymptotic regularization is obtained by solving the system of differential equations

$$\frac{d\mathbf{J}(t)}{dt} = -\mathbf{A}^T\mathbf{AJ}(t) + \mathbf{A}^T\mathbf{B}_z, \qquad [4]$$

where $\mathbf{A}^T$ is the transpose matrix of **A**, and t is an independent variable. The solution **J** asymptotically converges to the solution of Eq. [3], as $t \to \infty$.

The next step is to find the coil structure of the MRI magnet design. The coil has to be partitioned into a number of blocks, and each of them has a rectangular cross section. Initially, the number of the blocks are determined by number of oscillations in the solution **J**. Once an initial descretization of the coil geometry has been made, based on **J**, the structure must be refined. In principle, the magnetic field produced by a coil having many turns of wire can be computed in the same way as before. All that is required is to apply the Biot–Savart law, and integrate along each turn in the (short) solenoids. However, if a very large number of turns are involved, this procedure becomes prohibitively expensive for optimization. An alternative approach, which was proposed by Forbes *et al.* (*20* and references therein), is used for computing the magnetic field produced by a circular coil that contains a large number of turns wound onto a solenoid of rectangular cross section. Therefore, the magnetic field analysis is given as

$$\mathbf{B}(r, \theta, z) = \sum_{j=1}^{N} M_{rj}(r, \theta, z, R_j, \xi_j, w_j, h_j)I_0\hat{\mathbf{r}} + M_{zj}(r, \theta, z, R_j, \xi_j, w_j, h_j)I_0\hat{\mathbf{z}}, \qquad [5]$$

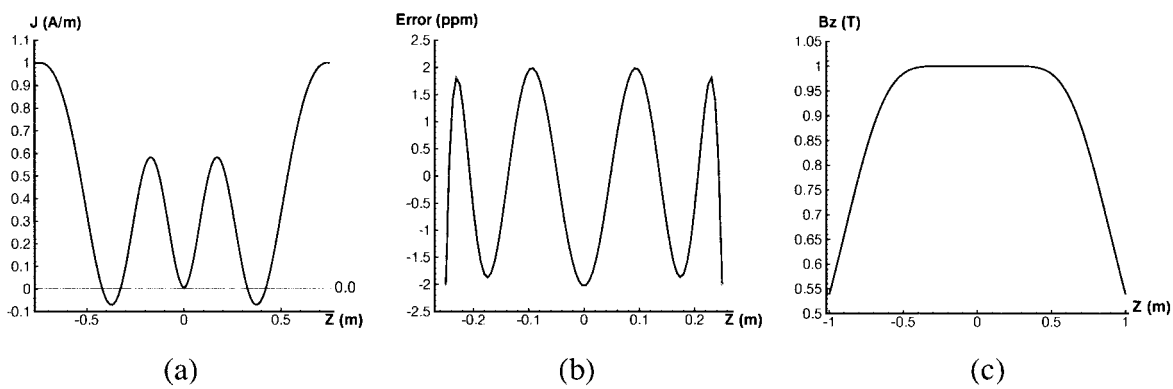

FIG. 2. A solution for a symmetric magnet: (a) the normalized current density distribution, (b) the error within dsv on the Z-axis, and (c) the normalized $\mathbf{B}_z$ field distribution on Z-axis.

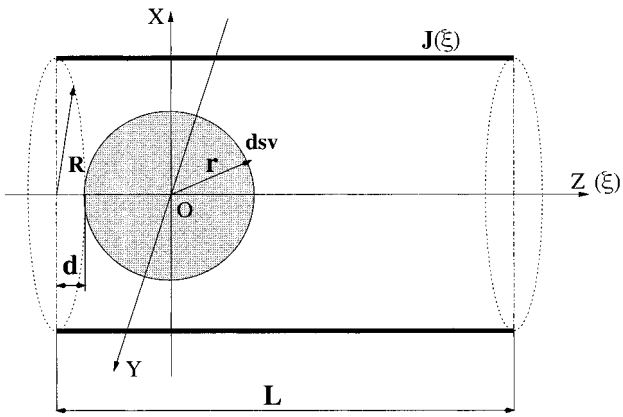

FIG. 3. An air-cored coil with an infinitely thin current density layer in an asymmetric magnet.

where N is the total number of the coils, (r, θ, z) is the field location, (R_j, ξ_j, w_j, h_j) are coordinates of the coil, M_r and M_z are the kernel of the summation that can be found in (*20*).

For nonlinear optimization design, the first step is to define a target field $\tilde{B}_z$ in a control region that can be chosen as the number of sample points $\tilde{B}_{zi}(r_i, \theta_i, z_i)$. Then, the problem becomes to search a solution set of $\mathbf{x} = (R_j, \xi_j, w_j, h_j; j = 1, 2, \ldots, N; I_0)$, where $\mathbf{x}$ is n dimensional vector $(n = 4N + 1)$. These solutions produce a field B_z that match the target field in the control region, that is

$$\begin{aligned} B_{zi}(\mathbf{r}_i) &= \sum_{j=1}^{N} M_{zj}(\mathbf{r}_i, x_{k+4(j-1)}, k = 1, \ldots, 4)\, x_{(4N+1)} \\ &= \tilde{B}_{zi}(\mathbf{r}_i), \quad i = 1, 2, \ldots, m, \end{aligned} \tag{6}$$

where m is the total number of control sample points, and $\mathbf{r}_i = (r_i, \theta_i, z_i)$. Equation [6] can be reranged as a system of the homogeneous equation

$$\begin{aligned} f_i(\mathbf{x}) &= \sum_{j=1}^{N} M_{zj}(\mathbf{r}_i, x_{k+4(j-1)}, k = 1, \ldots, 4)\, x_{(4N+1)} \\ &\quad - \tilde{B}_{zi}(\mathbf{r}_i) = 0, \quad i = 1, 2, \ldots, m \end{aligned} \tag{7}$$

with n unknown variables. In general, $m \geq n$ is chosen so that Eq. [7] is an over-determinate system. This nonlinear optimization problem can be solved as a nonlinear least squares problem; that is, let D be a solution space, $\mathbf{f}$: $D \subset R^n \rightarrow R^m$, $\mathbf{f} = (f_1, f, \ldots, f_m)^{\mathbf{T}}$, and define a function as

$$\Phi(\mathbf{x}) = \tfrac{1}{2}\, \mathbf{f}^{\mathbf{T}}(\mathbf{x})\mathbf{f}(\mathbf{x}), \quad \Phi\colon D \subset R^n \rightarrow R^1. \tag{8}$$

This function is the measure of the total difference between the target field and the field produced by the coils. The optimized $\mathbf{x}$ can be obtain by solving Eq. [8] for the minimum Φ value, that is

$$\min_{x \in D} \Phi(\mathbf{x}) = \min_{x \in D} \tfrac{1}{2}\, \mathbf{f}^{\mathbf{T}}(\mathbf{x})\mathbf{f}(\mathbf{x}). \tag{9}$$

The Levenberg–Marquardt method (*21*) is used that gives

$$[D\mathbf{f}^{\mathbf{T}}(\mathbf{x}^k)\, D\mathbf{f}(\mathbf{x}^k) + \alpha_k \mathbf{I}]\mathbf{p}_k(\alpha_k) = -D\mathbf{f}^{\mathbf{T}}(\mathbf{x}^k)\mathbf{f}(\mathbf{x}^k) \tag{10}$$

$$\mathbf{x}^{k+1} = \mathbf{x}^k + \lambda_k \mathbf{p}_k(\alpha_k), \tag{11}$$

where

$$D\mathbf{f}^{\mathbf{T}}(\mathbf{x}) = \begin{bmatrix} \dfrac{\partial f_1}{\partial x_1} & \dfrac{\partial f_2}{\partial x_1} & \cdots & \dfrac{\partial f_m}{\partial x_1} \\ \dfrac{\partial f_1}{\partial x_2} & \dfrac{\partial f_2}{\partial x_2} & \cdots & \dfrac{\partial f_m}{\partial x_2} \\ \vdots & \vdots & \ddots & \vdots \\ \dfrac{\partial f_1}{\partial x_n} & \dfrac{\partial f_2}{\partial x_n} & \cdots & \dfrac{\partial f_m}{\partial x_n} \end{bmatrix}, \tag{12}$$

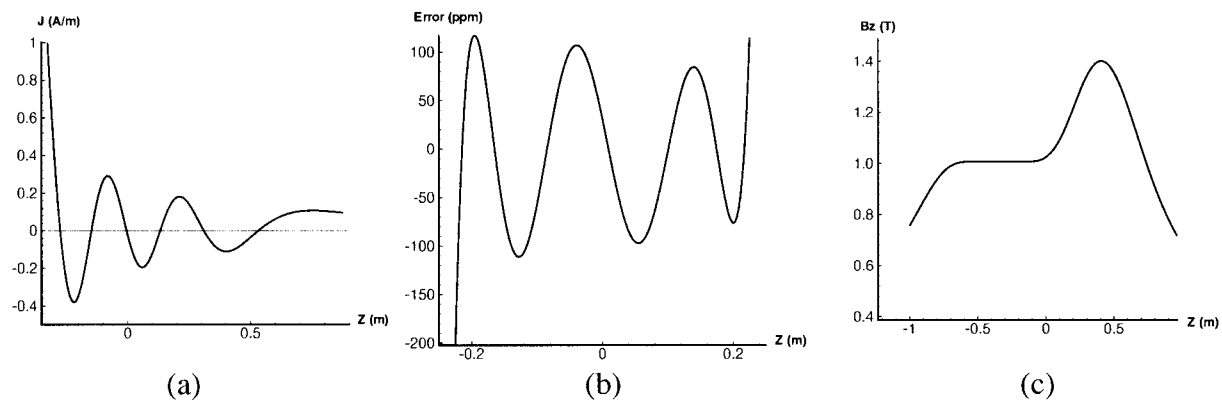

FIG. 4. A solution for the asymmetric magnet of design 1: (a) the normalized current density distribution, (b) the error within the dsv on the Z-axis, and (c) the normalized $\mathbf{B}_z$ field distribution on Z-axis.

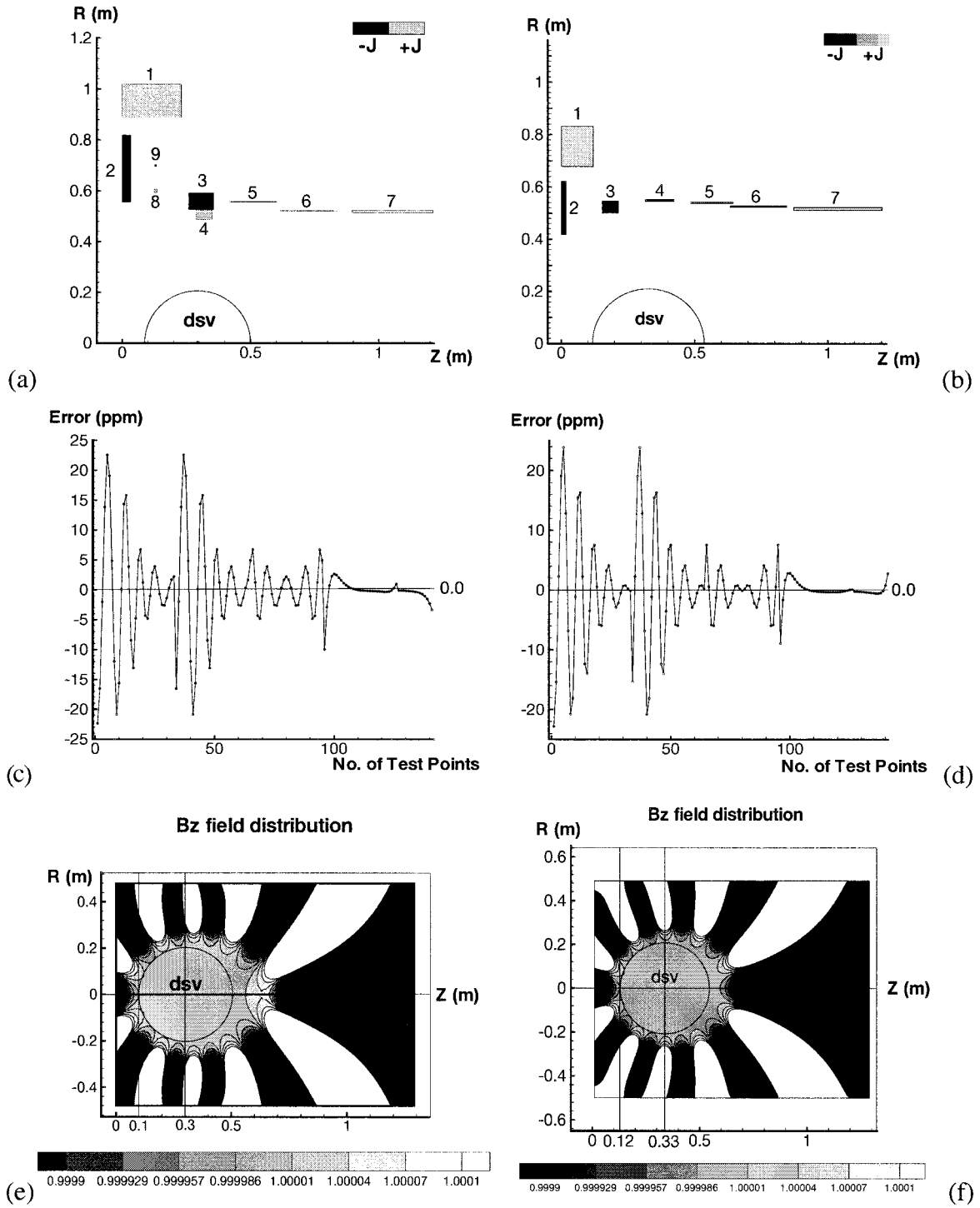

FIG. 5. Solutions for the example asymmetric magnets: (a) and (b) cross section of compact asymmetric magnet 1 and 2, respectively. Coils that are dark are counter-wound to the others; (c) and (d) the error over the complete dsv of magnet 1 and 2, respectively. (e) and (f) the $\mathbf{B}_z$ field distribution pattern relative to the dsv with 240 A transport current of magnet 1 and 2, respectively.

where $\alpha \geq 0$ is a damp factor, $\mathbf{I}$ is the identity matrix, $\mathbf{p}$ is the search direction, and λ is a parameter that can be found by using one-dimensional nonlinear optimization techniques. Equation [10] is an n-dimensional linear system. The LU decomposition method was used to solve for $\mathbf{p}$. The solution $\mathbf{x}$ is obtained when $\Phi(\mathbf{x}) \leq \epsilon$ is satisfied.

We first illustrate this method with a relatively unconstrained symmetric magnet example. The current density re-

TABLE 1
Asymmetric Magnet Design Results

	Design 1	Design 2
Total length (m)	1.2	1.2
Field strength (T)	1.0	1.0
Transport current (A)	240	240
Dsv (cm)		
40 epoch(cm)/Vrms(ppm)	9.0/2.8	13.0/3.2
45 epoch(cm)/Vrms(ppm)	7.5/7.0	11.5/8.2
50 epoch(cm)/Vrms(ppm)	4.0/19.0	8.0/22.0
Wire length (km)	130	64
Wire turns density (cm^{-2})	50.0	50.0
Peak field in superconductor (T)	8.2	8.0

quired is shown in Fig. 1. The overall length of the magnet is $L = 1.5$ m, the radius of the free bore is $R = 0.6$ m, and the radius of the dsv is $r = 0.25$ m. The relaxation factor is $\gamma = 0.833$. The field points $\mathbf{B}_{zj}$ were defined to be of constant value within the dsv. The solution was obtained with a maximum peak-to-peak error of about 2 ppm within the dsv along the *Z*-axis. The normalized current density distribution, the error profile, and the normalized $\mathbf{B}_z$ field distribution are given in Figs. 2a, 2b, and 2c, respectively. We note that the current density has a similar form to that seen by others (*23*).

As Fig. 2 shows, this approach results in a suitable current density profile, which generates a homogeneous $\mathbf{B}_z$ field on the axis. These results provide a very useful starting point for a coil wound design, in which the field over the complete dsv is considered. In the asymmetric case (see Fig. 3) two structures were designed. The overall length of each magnet was $L = 1.2$ m, the radius of the free bore was $R = 0.5$ m, and the radius of the dsv was $r = 0.21$ m. The relaxation factors were $\gamma = 0.18$ and $\gamma = 0.26$, respectively, corresponding to designs in which the dsv was positioned at either 9 or 13 cm from the end of the coil structure.

Figure 4 shows the final result of normalized continuous current density profile, the error, and the $\mathbf{B}_z$ field distributions on the *Z*-axis of the 10 cm dsv epoch magnet design. Since the γ in this case is much smaller than in the symmetric case, the maximum error eventually only converged to about 200 ppm peak-to-peak within the dsv. However, this solution still provides enough information to allow an initial coil pattern to be established. Nonlinear optimization or the simulated annealing method may then be used to refine the coil structure. It is interesting to note (see Figs. 2c and 4c) that the principal impurities in the symmetric design are of even order, while those in the asymmetric case possess odd symmetry.

The continuous current density function shown in Fig. 4a is clearly oscillating positively and negatively. According to these distributions, at least $l = 7$ coils are needed for magnet structure to reasonably approximate the continuous current distribution. Each coil has 4 parameters to be determined, the coordinates of the center, width, inner radius, and height of the block. For the convenience of initial design, the same turns density was used for all the coils (0.5 mm^{-2}) and constant transport current assumed. The constant target field ($\mathbf{B}_{ztag}$) was set to 1.0 T. For the case presented here, the sample points ($m = 150$) evenly spaced over the dsv and including its surface were selected and the algorithm set a target to reduce the peak-to-peak error within the dsv to less than 10 ppm.

Since the initial values of the coil dimensions and position were determined from a continuous current density profile, we make the assumption that the initial set of **x** were in the domain of the globe minimum. This has been confirmed by running several Simulated Annealing algorithms on the initial values to ensure that they are in the vicinity of the global minimum. The nonlinear method then descends to the optimal solution. Furthermore, the current density distributions shown from Fig. 4 only guarantee the homogeneity of the $\mathbf{B}_z$ field on the *Z*-axis within dsv. When our nonlinear optimization technique was used for resizing the discrete coils for $\mathbf{B}_z$ generation over the entire dsv, the solution was, not surprisingly, different from that when only the *Z*-axis fields were considered. The solutions, however, have the same general topology, indicating the advantage of using the initial current density approximation. Computation times for asymmetric designs were approximately 3–4 min for the current density calculations and up to

TABLE 2
Coil Configurations in Meters

	Design 1					Design 2				
	R1	R2	Z1	Z2	**J**	R1	R2	Z1	Z2	**J**
Coil 1	0.888647	1.019661	0.000000	0.230233	+	0.678349	0.831083	0.000000	0.120118	+
Coil 2	0.556452	0.819145	0.000000	0.033506	−	0.417993	0.622359	0.000000	0.017729	−
Coil 3	0.527031	0.592246	0.259035	0.355951	−	0.500673	0.546588	0.153321	0.213309	−
Coil 4	0.487356	0.524118	0.287825	0.349032	+	0.545729	0.552018	0.314059	0.422412	−
Coil 5	0.555548	0.557867	0.418295	0.602217	−	0.537916	0.542539	0.485078	0.643620	+
Coil 6	0.521077	0.521786	0.615035	0.841080	−	0.523675	0.526570	0.633419	0.845569	+
Coil 7	0.514972	0.523409	0.895588	1.212376	+	0.510686	0.521938	0.872007	1.202192	+
Coil 8	0.593770	0.605756	0.123928	0.135913	+					
Coil 9	0.698071	0.701878	0.128102	0.131917	+					

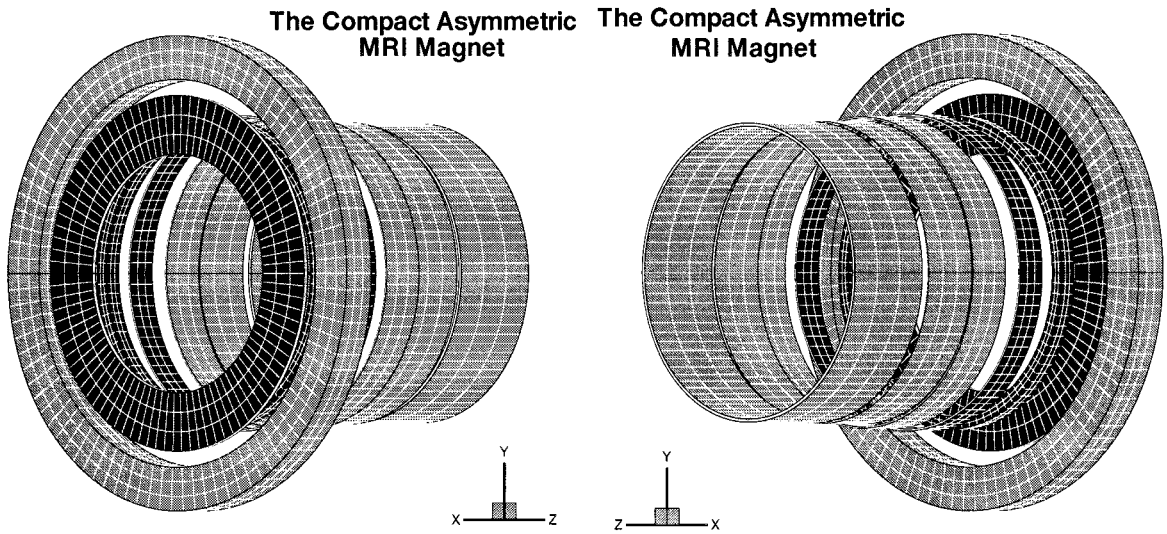

FIG. 6. The compact asymmetric MRI magnet.

8 h for the block optimization when implemented on an SGI Origin 2000.

Figure 5 illustrates the final results for the compact asymmetric MRI magnet designs, Table 1 summarizes their properties, and Table 2 shows the detail configuration of each coil for both designs. In all cases, the final V_{rms} values on the dsv were calculated using 600 points to ensure over sampling.

While both magnets produce useful fields (see Fig. 5), design 2 is much more economical and is therefore preferred. This is a consequence of attempting to force the dsv epoch to be very near the magnet end and results in large cancellation fields and excessive wire lengths. Design 2 has a volume rms of about 8 ppm over a dsv of 45 cm, the epoch of which is 11.5 cm from the end of the magnet. The magnet structure is buildable and the peak fields and current densities are within working limits of NbTi conductors. The energy storage of design 2 is approximately 5.9 MJ.

A conventional, symmetric magnet of 1.2 m (*14*) requires only 41 km of wire, the additional wire costs of design 2 being due to its strong asymmetry. As the dsv moves closer to the geometric center of the magnet structure the wire costs reduce. The contour plot of Fig. 5f illustrates the position and purity of dsv. Figure 6 provides a perspective view of the final magnet structure. In this figure, darkly shaded coils are counter-wound to all others. It is instructive to compare the asymmetric design to a symmetric design of similar dsv size and epoch. A 67 cm long symmetric system, designed using our approach, requires approximately 112 km of wire and has a resultant purity of about 20 ppm V_{rms} over a 45 cm dsv. The asymmetric system is thus preferable to this system in both cost and dsv purity. Asymmetric gradient coils would, of course, be used in the asymmetric magnets and potentially there would be a reduction in the volumetric $\partial \mathbf{B}/\partial t$ exposure and hence in peripheral nerve stimulation.

In summary, a hybrid numerical method has been successfully applied to the design of new, compact, asymmetric MRI magnets. This method is flexible and may be applied to magnets of other geometries. A design was detailed which allowed a 45 cm dsv to begin only 11 cm away from one end of the magnet with overall length 1.2 m. In this magnet, most of the patient will remain outside the magnet structure allowing significantly improved physician access and reduced perception of claustrophobia in many cases. We note that in a cardiac examination, for example, the patient's head would be outside the magnet structure. While this work has focused on single-layer current densities and coil implementations thereof, the method is extendable to multilayer current densites which may be used for multiple primaries or for shielding windings.

ACKNOWLEDGMENT

The authors gratefully acknowledge support for this project from The Australian Research Council.

REFERENCES

1. M. W. Garrett, *J. Appl. Phys.* **22,** 1091 (1951).
2. M. W. Garrett, *J. Appl. Phys.* **34,** 2567 (1963).
3. M. W. Garrett, *J. Appl. Phys.* **38,** 2563 (1967).
4. H. Saint-Jalmes, J. Taquin, and Y. Barjhoux, *Rev. Sci. Instrum.* **52,** 1501 (1981).
5. H. Siebold, H. Huebner, L. Soelsner, and T. Reichert, *IEEE Trans. Magn.* **24,** 419 (1988).
6. K. Schweikert, R. Kreig, and F. Noack, *J. Magn. Reson.* **78,** 77 (1988).
7. H. Siebold, *IEEE Trans. Magn.* **26,** 841 (1990).
8. F. J. Davies, R. T. Elliott, and D. G. Hawkesworth, *IEEE Trans. Magn.* **27,** 1677 (1991).
9. A. K. Kalafala, *IEEE Trans. Magn.* **27,** 1696 (1991).

10. W. M. Schmidt, R. R. Huson, W. W. Mackay, and R. M. Rocha, *IEEE Trans. Magn.* **27,** 1681 (1991).

11. S. Pissanetzky, *IEEE Trans. Magn.* **28,** 1961 (1992).

12. M. R. Thompson, R. W. Brown, and V. C. Srivastava, *IEEE Trans. Magn.* **30,** 108 (1994).

13. S. Noguchi and A. Ishiyama, *IEEE Trans. Magn.* **33,** 1904 (1997).

14. S. Crozier and D. M. Doddrell, *J. Magn. Reson.* **127,** 233 (1997).

15. P. N. Morgan, S. Conolly, and A. Macovski, *Magn. Reson. Med.* **41,** 1221 (1999).

16. R. Turner and R. M. Bowley, *J. Phys. E.* **19,** 876 (1986).

17. P. Mansfield and B. Chapman, *J. Phys. E.* **19,** 540 (1986).

18. D. Hoult and R. Deslauriers, *J. Magn. Reson.* **108,** 9 (1994).

19. J. D. Jackson, "Classical Electromagnetics," Wiley, New York (1975).

20. L. K. Forbes, S. Crozier, and D. M. Doddrell, *IEEE Trans. Magn.* **33,** 4405 (1997).

21. W. H. Press, S. A. Teukolsky, W. T. Vetterling, and B. P. Fannery, "Numerical Recipes in C," Cambridge Univ. Press, Cambridge, UK (1989).

22. M. Guarnieri, A. Stella, and F. Trevisan, *IEEE Trans. Magn.* **26,** 622 (1990).

23. R. Brown, H. Fujita, S. M. Shvartsman, M. R. Thompson, M. A. Morich, L. S. Petropolous, and V. C. Srireastarea, *Int. J. Appl. Elect.* **9,** 277 (1998).